Dynamics of Polar Skyrmion Bubbles under Electric Fields

Ruixue Zhu,[1,*] Zhexin Jiang,[2,*] Xinxin Zhang,[1,*] Xiangli Zhong,[3,*] Congbing Tan,[4,†] Mingwei Liu,[4] Yuanwei Sun,[1] Xiaomei Li,[1,5] Ruishi Qi,[1] Ke Qu,[1] Zhetong Liu,[1] Mei Wu,[1] Mingqiang Li,[1] Boyuan Huang,[7] Zhi Xu,[5] Jinbin Wang,[3] Kaihui Liu,[9,10] Peng Gao,[1,10,‡] Jie Wang,[2,8,§] Jiangyu Li,[6] and Xuedong Bai[5,11,‖]

[1]*Electron Microscopy Laboratory and International Center for Quantum Materials, School of Physics, Peking University, Beijing 100871, China*

[2]*Department of Engineering Mechanics, Zhejiang University, Hangzhou 310027, Zhejiang, China*

[3]*School of Materials Science and Engineering, Xiangtan University, Xiangtan 411105, Hunan, China*

[4]*Hunan Provincial Key Laboratory of Intelligent Sensors and Advanced Sensor Materials, School of Physics and Electronics, Hunan University of Science and Technology, Xiangtan 411201, Hunan, China*

[5]*Beijing National Laboratory for Condensed Matter Physics, Institute of Physics, Chinese Academy of Sciences, Beijing 100190, China*

[6]*Guangdong Provincial Key Laboratory of Functional Oxide Materials and Devices, Southern University of Science and Technology, Shenzhen 518055, Guangdong, China*

[7]*Department of Materials Science and Engineering, Southern University of Science and Technology, Shenzhen 518055, Guangdong, China*

[8]*Zhejiang Laboratory, Hangzhou 311100, Zhejiang, China*

[9]*State Key Laboratory for Artificial Microstructure & Mesoscopic Physics, School of Physics, Peking University, Beijing 100871, China*

[10]*Interdisciplinary Institute of Light-Element Quantum Materials and Research Center for Light-Element Advanced Materials, Peking University, Beijing, 100871, China*

[11]*School of Physical Sciences, University of Chinese Academy of Sciences, Beijing 100049, China*

(Received 9 August 2021; revised 23 June 2022; accepted 11 August 2022; published 2 September 2022)

Room-temperature polar skyrmions, which have been recently discovered in oxide superlattice, have received considerable attention for their potential applications in nanoelectronics owing to their nanometer size, emergent chirality, and negative capacitance. For practical applications, their manipulation using external stimuli is a prerequisite. Herein, we study the dynamics of individual polar skyrmions at the nanoscale via *in situ* scanning transmission electron microscopy. By monitoring the electric-field-driven creation, annihilation, shrinkage, and expansion of topological structures in real space, we demonstrate the reversible transformation among skyrmion bubbles, elongated skyrmions, and monodomains. The underlying mechanism and interactions are discussed in conjunction with phase-field simulations. The electrical manipulation of nanoscale polar skyrmions allows the tuning of their dielectric permittivity at the atomic scale, and the detailed knowledge of their phase transition behaviors provides fundamentals for their applications in nanoelectronics.

DOI: 10.1103/PhysRevLett.129.107601

Topological polar structures [1–4], such as vortices [5–10], antivortices [11,12], flux closures [13–16], skyrmion bubbles [1,17], merons [18], and toroidal topological textures [19] that are the electric analogs of magnetic topologies, have recently been discovered in low-dimensional ferroelectrics and oxide superlattices. Because of the strong dielectric anisotropy in polar systems, significant energy is required to deviate the electric dipoles from the crystallographic polar axes; this makes the formation of polar topologies difficult [20–23]. Particlelike polar topologies are stabilized by the complex interplay among elastic, electrostatic, and gradient energies, and they exhibit exotic properties, like negative capacitance [24,25] and chirality [1,26–28], that make them promising candidates for robust, ultralow-power-consumption and high-density nanoelectronic devices in the post-Moore era.

Most applications require the ability to tune polar states and require the knowledge of their phase transition behaviors under external stimuli. Several theoretical and experimental studies have analyzed the phase transition pathways of polar topological defects under various external stimuli. For example, an electric field or stress can alter the delicate balance between the depolarization field and strain boundary condition; thus, flux closures and vortices can reversibly change between topological and trivial ferroelectric states [29–33]. An ultrafast optical pulse promotes the transformation of the polar vortice and a_1/a_2 domain mixture to the long-range supercrystal phase [34]. Additionally, polar vortices exhibit collective dynamic behavior under the subterahertz field [35].

Upon heating, polar skyrmions can undergo topological phase transition according to Landau theory [36] and can

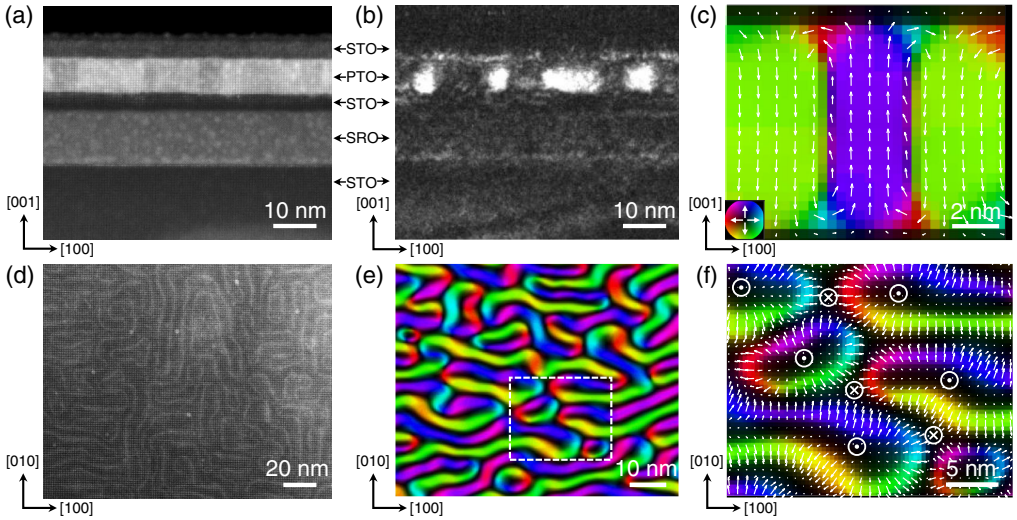

FIG. 1. Observation of mixed skyrmion bubbles and elongated skyrmions. (a) Cross-sectional MAADF image of the $(SrTiO_3)_{11}/(PbTiO_3)_{22}/(SrTiO_3)_{11}$ trilayer sample, and (b) a dark-field TEM image, displaying an alternating high and low diffraction contrast within the PTO layer. (c) Antiparallel polarization distribution of the cross-sectional view from phase-field simulations (denoted by white arrows). The background color mapping illustrates the polarization orientation. (d) Planar-view MAADF-STEM image showing the coexistence of skyrmion bubbles and elongated skyrmions. For these domains, dark regions possessing out-of-plane polarization are separated by bright domain walls with in-plane polarization. (e) Low-magnification and (f) enlarged view of the white dashed box color mappings constructed from phase-field simulations, depicting the in-plane polarization distribution with hedgehog-like features. The background color saturation is proportional to the in-plane polarization magnitude; i.e., in the dark regions, in-plane polarization is basically null while the out-of-plane polarization is dominant, representing the core or periphery of polar skyrmions. The symbols circle cross and circle dot denote downward and upward polarizations, respectively.

even form an intermediate state, the meron, with half the topological number [37]. Furthermore, theoretical studies [38–40] have predicted that the phase transition between topological polar skyrmions and trivial ferroelectric phase can occur at room temperature, which is highly desired for most nanoelectronic applications. Experimentally, macroscopic dielectric measurements and x-ray diffraction reciprocal space mappings have detected the response of polar skyrmions to electric fields and observed the topological phase transition [24], during which considerable tunability of the dielectric permittivity was achieved. However, considering practical applications, the evolution of individual polar skyrmions with different sizes and their interactions with each other under external fields need to be understood; this has motivated this study, which analyzes the dynamic behavior of polar skyrmions at the nanoscale in the real space.

Herein, we directly observe the electric-field-driven evolution of individual polar skyrmions via *in situ* scanning transmission electron microscopy (STEM). We determine that polar skyrmion bubbles can be created by fragmenting the pristine elongated skyrmions under an electric field. Further increasing the field leads to their shrinkage and annihilation, forming a trivial monodomain. In contrast, an opposite bias causes their expansion, interaction, and merger into a monodomain. Upon returning to zero bias, isolated skyrmion bubbles randomly renucleate within the monodomain. The multistate switching among skyrmion bubbles, elongated skyrmions, and monodomain is reversible and repeatable. Thus, electric fields can be used to tune the state of polar skyrmions at room temperature and polar-skyrmion-based nanodevices can be designed.

The low-magnification medium angle annular dark field (MAADF)-STEM image in Fig. 1(a) shows a $(SrTiO_3)_{11}/(PbTiO_3)_{22}/(SrTiO_3)_{11}$ trilayer film grown on a $SrTiO_3$ (STO) (001) single crystal substrate via pulsed laser deposition, with a $SrRuO_3$ (SRO) conductive layer in the middle serving as the bottom electrode (see Methods for details). The cross-sectional MAADF image in Fig. 1(a) and the dark-field image under two beam conditions in Fig. 1(b) (and Fig. S1 of the Supplemental Material [41]) display the nonuniform diffraction contrast in the $PbTiO_3$ (PTO) layer, which originates from local strain field [42] around polar skyrmions (Figs. S2 and S3). The alternating bright and dark regions reflect the antiparallel out-of-plane polarization, as shown in the simulated polarization mapping [Fig. 1(c)]. The planar-view image [Fig. 1(d)] further suggests the coexistence of circular skyrmion bubbles with elongated skyrmions, which well matches the previous study [1]. Moreover, such a mixed structure can be well reproduced using phase-field simulations [Figs. 1(e) and 1(f)], wherein the colorful domain walls with in-plane polarization correspond to the bright stripes in Fig. 1(d). The diffraction contrast of bright stripes is derived from in-plane lattice distortion. Figure S2 [41] displays the configuration of three-dimensional electric dipole distribution

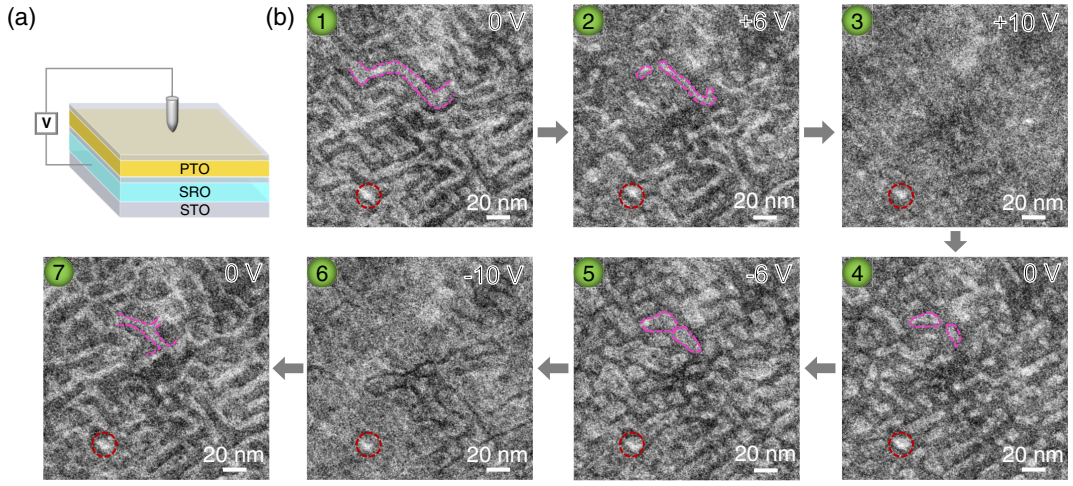

FIG. 2. Electrical switching dynamics of polar skyrmions in a trilayer. (a) Schematic showing the experimental setup of *in situ* STEM. A tungsten tip and SRO conductive layer are used as electrodes to apply an out-of-plane electric field to the film. (b) Selected snapshots showing the evolution of elongated skyrmions and skyrmion bubbles under positive and negative bias loading periods. The threshold electric field is ~5682 kV/cm (10 V). Purple dashed lines outline the characteristic domains. Red circles indicate the drift correction positions. Each frame is processed using principal component analysis for better visualization.

for a single skyrmion bubble, with the topological number $N_{sk} = +1$ in each plane:

$$N_{sk} = \frac{1}{4\pi} \iint \boldsymbol{n} \cdot \left(\frac{\partial n}{\partial x} \times \frac{\partial n}{\partial y} \right) dxdy, \tag{1}$$

where **n** denotes the normalized electric dipole moment vector and (x, y) denote the spatial position [50,51].

To determine the dynamic evolution of polar skyrmions under an applied electric field, we use a tungsten probe and the conductive SRO layer as electrodes to apply an out-of-plane electric field to the film in the electron microscope [Fig. 2(a)]. We perform *in situ* experiments in the STEM mode along the $[01\bar{2}]$ zone axis for better contrast (Fig. S4). Figure 2(b) displays several typical snapshots of dynamic evolution selected from movie S1, in the Supplemental Material [41]. We first apply a positive bias to the trilayer, which is downward and antiparallel to the skyrmion core polarization. When the bias is increased from 0 to +6 V, the elongated skyrmions shrink and shorten, becoming thinner and smaller. Some elongated skyrmions are fragmentized into isolated skyrmion bubbles, as outlined in purple in Fig. 2(b) and Fig. S5 [41]. As the positive bias further increases, the newly formed bubbles and residual elongated skyrmions transition to the downward-poled monodomain. Herein, most of skyrmions disappear when the bias is ~10 V and N_{sk} changes from +1 to 0. However, the accurate critical bias is difficult to quantitively estimate due to the complicated contact geometry in the *in situ* experimental setup. Nevertheless, our phase-field simulations provide a reference value ~12.6 V, which is comparable with the experiment. Such an electric-field-stabilized ferroelectric monodomain is metastable. After removing the positive bias, considerable isolated skyrmions spontaneously return.

Continuing to apply a negative bias, the driving force widens skyrmion bubbles and elongated skyrmions, eventually coalescing into an upward-poled monodomain. Notably, many dark stripes are still present when the bias is −10 V, indicating an incomplete topological phase transition, and the actual threshold is greater than −10 V. Furthermore, this monodomainlike state at −10 V is metastable, i.e., the mixed structure regenerates to a state similar to the initial state when the bias is removed, demonstrating reversibility. Such asymmetric cyclic switching of polar skyrmions signifies hysteretic behavior (Fig. S6), which is quite common in ferroelectric thin films [52,53]. The measured bright domains under the electric bias cycle exhibit a ferroelectric loop and an obvious negative horizontal shift; this is because of the differences in nonuniform electric field caused by the asymmetric electrode shapes and/or Schottky barriers at the interfaces [54,55].

We simulate the dynamic evolution of coexisting polar skyrmions by applying a homogeneous out-of-plane electric field in the phase-field simulations. The in-plane polarization evolution in Fig. 3 verifies the intermediate process, where elongated skyrmions gradually shrink and some break into bubbles with increasing electric field (white dashed boxes in Fig. 3 and Fig. S7 [41]), which agrees with the experimental results. Topological phase transition occurs under a critical voltage of $U_{[001]} =$ 12.6 V, whereupon all the topological domains disappear and saturate into a uniform monodomain. Additionally, N_{sk} becomes zero. The simulations confirm that a similar recovery from monodomain to a mixture of skyrmions occurs when the bias is decreased to 0 V, indicating the

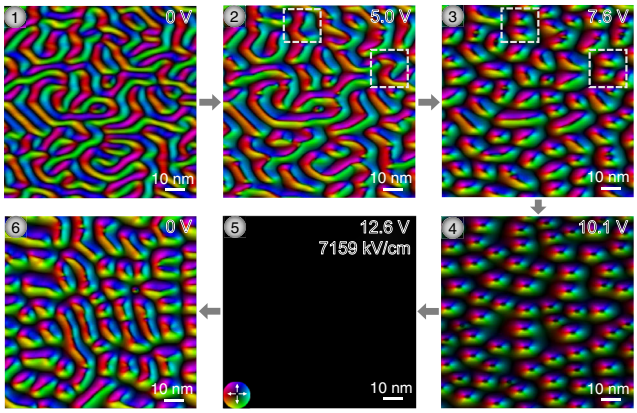

FIG. 3. Evolution of the coexisting structure in the trilayer under an external electric field from phase-field simulations. The first five frames display the topological phase transition from polar skyrmions to the trivial monodomain that is induced by an out-of-plane electric field. A uniform saturated monodomain forms under a critical voltage of $U_{[001]} = 12.6$ V ($E_{[001]} = 7159$ kV/cm). The sixth frame displays the relaxation process after the removal of the external field. White dashed boxes highlight domains with fracture characteristics.

lower energy of the mixed state. When the voltage is further decreased, skyrmion bubbles appear to elongate and widen through the motion of 180° domain walls. Figure S7 displays the evolution of electric dipoles under the opposite voltages. Notably, during the expansion, 180° domain walls with antiparallel electric dipoles in adjacent skyrmions gradually approach each other, causing a sharp increase in the strength of Coulomb repulsive interactions, thereby preventing coalescence and forming another 'counterclockwise' type polar skyrmion [Figs. S7(d) and S10].

For comparison, we probe the dynamic behavior of polar skyrmions in the $[(SrTiO_3)_{11}/(PbTiO_3)_{22}/(SrTiO_3)_{11}]_6$ superlattice, which possesses a high density of small-sized bubbles according to a previous study [1]. Indeed, the MAADF image of cross section in Fig. 4(a), the corresponding dark-field image in Fig. S8, and the planar-view STEM image in Fig. 4(b) confirm the presence of numerous isolated bubbles and the elongated skyrmions are short and few. Notably, these topological domains can extend through lattice defects and are almost unaffected by them [Fig. 4(b)]. For the positive branch shown in Fig. 4(c), a topological phase transition is observed when the bias is increased from 0 to 6 V. Some smaller bubbles start disappearing even at a bias of 4 V (indicated by orange arrows), while the larger ones gradually shrink and then vanish (indicated by yellow arrows), in agreement with the previous simulation [24]. When the external stimuli is removed, skyrmion bubbles spontaneously reappear. A similar expansion is observed in the negative branch with a critical bias of about −10 V, which is greater than the positive threshold. Such similar asymmetric switching is also likely due to the asymmetric electrodes (movie S2 and Fig. S9). Furthermore, the analogous evolution of

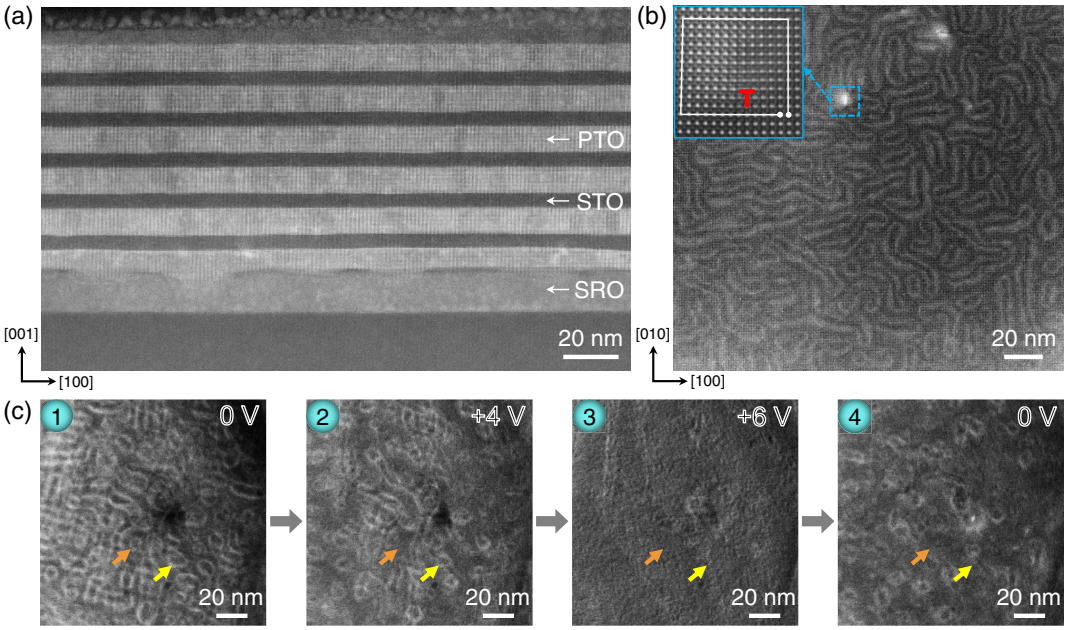

FIG. 4. Electrical switching dynamics of polar skyrmions in a superlattice. (a) Cross-sectional and (b) planar-view MAADF-STEM images of the superlattice $[(SrTiO_3)_{11}/(PbTiO_3)_{22}/(SrTiO_3)_{11}]_6$. The enlarged view of the blue dashed box in (b) is placed in the upper left corner, exhibiting an edge dislocation with **a**[100] burgers vector. (c) Evolution of skyrmion bubbles under a positive bias loading along the [001] zone axis. Threshold electric field is about ~3409 kV/cm (6 V). For better visualization, the background in images 1–4 is removed (see Fig. S9 for original images [41]). The characteristic polar skyrmions during the shrinkage process are indicated by orange and yellow arrows.

elongated skyrmions in the superlattice (Fig. S11) demonstrates the repeatability of the phase transition.

Thus far, our *in situ* experiments on the $(SrTiO_3)_{11}/(PbTiO_3)_{22}/(SrTiO_3)_{11}$ trilayer and superlattice mainly reveal the reversible transformation among skyrmion bubbles, elongated skyrmions and monodomain in the real space, which corroborate the recently published simulation results and experiments in the reciprocal space [24,39,40]. Two major reversible processes are present: First, the switching between polar skyrmions and monodomain signifies that these topological solitons can be eliminated and generated using an electric field. Second, the switching between skyrmion bubbles and elongated skyrmions illustrates the size adjustability of polar skyrmions. Since mixed polar skyrmions are nonuniform in shape and size at nanometer level, their evolution details cannot be clarified in reciprocal space [24].

The intermediate states and interactions of polar skyrmions can be further analyzed. During the shrinkage process, the so-called "blowing" skyrmion bubbles from the elongated skyrmions is noteworthy [39,56], which is similar to the "nanodomains ejection from domain walls" reported in a previous study [57]. The evolution mechanism can be well understood from the energy perspective, i.e., the applied downward electric field can break the degeneracy of the double-well potential and modify the energy profile as shown in Fig. S12(a), resulting in an energy increase of polarizations antiparallel to the electric field. In order to effectively decrease the electric energy [Fig. S12(b)], polar skyrmions tend to shrink to reduce the area ratio of the upward polarized domains. Similarly, the upward electric field promotes the expansion of skyrmions, during which 180° domain walls of the adjacent skyrmion #A and #B approach each other (Fig. S10). Meanwhile, the antiparallel polar vectors (denoted by black arrows) create repulsive Coulomb interactions, preventing domain walls from further approaching. The trade-off of these two mechanisms favors the formation of another counterclockwise skyrmion #C. Analogously, the newly formed skyrmions disappear after the driving force crosses the finite energy barrier between topological and trivial ferroelectric states.

Another noteworthy issue is whether polar skyrmions have long-range motion when excited using an electric field. Herein, the "center" position of polar skyrmions is basically unchanged during the *in situ* experiments driven by only a single out-of-plane electric bias; however, the regenerated positions of skyrmions can be slightly different from the original ones after the electric field is removed. Reminiscent of the in-plane spin-polarized current that can drive the motion of magnetic skyrmions [58,59], we employ phase-field simulations to apply an in-plane electric field (see Fig. S13). However, in contrast to the magnetic case, all polar skyrmions disappear under a small in-plane voltage rather than the expected overall long-range motion. Thus, moving polar skyrmions using simple electric fields seems difficult.

In summary, our study experimentally revealed the electrically driven dynamic behaviors of polar skyrmions at the nanoscale. By applying an electric field with proper direction and magnitude, we can create, erase, or change the size of polar skyrmions. The evolution of polar skyrmions under an out-of-plane electric field is similar to that of magnetic analogs driven by a magnetic field [56,60], showing a transition between elongated skyrmions to bubbles and then to monodomains, except that the polar skyrmions do not exhibit any obvious long-range motion, even when an in-plane electric field is applied. Additionally, observations in real space directly display intermediate states in the reversible conversion and interactions between different topological individuals, as well as the effect of lattice defects. Furthermore, the enriched microstructural information lays the foundation for interpreting the macroscopic performance, including asymmetric curves of permittivity under opposite electric fields [24]. This electrically driven method for generating more and smaller skyrmion bubbles from the mixed structure is simpler and more effective than the layer tuning suggested in the previous study [1]. Thus, real space observations of the tunable behaviors of topological polar skyrmions under an electric field provide vital information for their potential applications in nanoelectronics [41].

This research was supported by the National Natural Science Foundation of China (No. 12104017, No. 52125307, No. 11974023, No. 52021006, No. T2188101, No. 11972320, No. 52025023, No. 51991344), the Key R&D Program of Guangdong Province (No. 2018B030327001, No. 2018B010109009, No. 2020B010189001, No. 2019B010931001), the Program of Chinese Academy of Sciences (No. XDB33030200, No. ZDYZ2015-1), and the "2011 Program" from the Peking-Tsinghua-IOP Collaborative Innovation Center of Quantum Matter, and the Pearl River Talent Recruitment Program of Guangdong Province (No. 2019ZT08C321). And we acknowledge the support of the Guangdong Provincial Key Laboratory Program (No. 2021B1212040001) from the Department of Science and Technology of Guangdong Province and the support of the Key Research Project from Zhejiang Laboratory (No. 2021 PE0AC02). We also thank the Electron Microscopy Laboratory in Peking University for the use of the Cs-corrected electron microscope.

[*]These authors contributed equally to this work.
[†]Corresponding author.
cbtan@xtu.edu.cn
[‡]Corresponding author.
p-gao@pku.edu.cn
[§]Corresponding author.
jw@zju.edu.cn
[‖]Corresponding author.
xdbai@iphy.ac.cn

[1] S. Das *et al.*, Observation of room-temperature polar skyrmions, Nature (London) **568**, 368 (2019).

[2] Y. Tang, Y. Zhu, B. Wu, Y. Wang, L. Yang, Y. Feng, M. Zou, W. Geng, and X. Ma, Periodic polarization waves in a strained, highly polar ultrathin $SrTiO_3$, Nano Lett. **21**, 6274 (2021).

[3] F.-H. Gong *et al.*, Atomic mapping of periodic dipole waves in ferroelectric oxide, Sci. Adv. **7**, eabg5503 (2021).

[4] L. Lu *et al.*, Topological Defects with Distinct Dipole Configurations in $PbTiO_3/SrTiO_3$ Multilayer Films, Phys. Rev. Lett. **120**, 177601 (2018).

[5] A. K. Yadav *et al.*, Observation of polar vortices in oxide superlattices, Nature (London) **530**, 198 (2016).

[6] S. L. Hsu, M. R. McCarter, C. Dai, Z. Hong, L. Q. Chen, C. T. Nelson, L. W. Martin, and R. Ramesh, Emergence of the vortex state in confined ferroelectric heterostructures, Adv. Mater. **31**, e1901014 (2019).

[7] Y. Sun *et al.*, Subunit cell-level measurement of polarization in an individual polar vortex, Sci. Adv. **5**, eaav4355 (2019).

[8] Z. Hong *et al.*, Stability of polar vortex lattice in ferroelectric superlattices, Nano Lett. **17**, 2246 (2017).

[9] B. Rodriguez, X. Gao, L. Liu, W. Lee, I. Naumov, A. Bratkovsky, D. Hesse, and M. Alexe, Vortex polarization states in nanoscale ferroelectric arrays, Nano Lett. **9**, 1127 (2009).

[10] W. Wang, Y. Zhu, Y. Tang, Y. Xu, Y. Liu, S. Li, S. Zhang, Y. Wang, and X. Ma, Large scale arrays of four-state vortex domains in $BiFeO_3$ thin film, Appl. Phys. Lett. **109**, 202904 (2016).

[11] A. Y. Abid *et al.*, Creating polar antivortex in $PbTiO_3/SrTiO_3$ superlattice, Nat. Commun. **12**, 2054 (2021).

[12] J. Kim, M. You, K.-E. Kim, K. Chu, and C.-H. Yang, Artificial creation and separation of a single vortex–antivortex pair in a ferroelectric flatland, npj Quantum Mater. **4**, 29 (2019).

[13] Y. Tang *et al.*, Observation of a periodic array of flux-closure quadrants in strained ferroelectric $PbTiO_3$ films, Science **348**, 547 (2015).

[14] Y. Liu, Y.-J. Wang, Y.-L. Zhu, C.-H. Lei, Y.-L. Tang, S. Li, S.-R. Zhang, J. Li, and X.-L. Ma, Large scale two-dimensional flux-closure domain arrays in oxide multilayers and their controlled growth, Nano Lett. **17**, 7258 (2017).

[15] S. Li, Y. Zhu, Y. Wang, Y. Tang, Y. Liu, S. Zhang, J. Ma, and X. Ma, Periodic arrays of flux-closure domains in ferroelectric thin films with oxide electrodes, Appl. Phys. Lett. **111**, 052901 (2017).

[16] C.-L. Jia, K. W. Urban, M. Alexe, D. Hesse, and I. Vrejoiu, Direct observation of continuous electric dipole rotation in flux-closure domains in ferroelectric $Pb(Zr,Ti)O_3$, Science **331**, 1420 (2011).

[17] J. Yin *et al.*, Nanoscale bubble domains with polar topologies in bulk ferroelectrics, Nat. Commun. **12**, 3632 (2021).

[18] Y. J. Wang *et al.*, Polar meron lattice in strained oxide ferroelectrics, Nat. Mater. **19**, 881 (2020).

[19] M. Guo *et al.*, Toroidal polar topology in strained ferroelectric polymer, Science **371**, 1050 (2021).

[20] G. Catalan, J. Seidel, R. Ramesh, and J. F. Scott, Domain wall nanoelectronics, Rev. Mod. Phys. **84**, 119 (2012).

[21] A. S. Sidorkin, *Domain Structure in Ferroelectrics and Related Materials* (Cambridge International Science, Cambridge, England, 2006).

[22] Q. Jiang, E. Subbarao, and L. Cross, Grain size dependence of electric fatigue behavior of hot pressed PLZT ferroelectric ceramics, Acta Metall. Mater. **42**, 3687 (1994).

[23] C. Kittel, Theory of the structure of ferromagnetic domains in films and small particles, Phys. Rev. **70**, 965 (1946).

[24] S. Das *et al.*, Local negative permittivity and topological phase transition in polar skyrmions, Nat. Mater. **20**, 194 (2021).

[25] A. K. Yadav *et al.*, Spatially resolved steady-state negative capacitance, Nature (London) **565**, 468 (2019).

[26] P. Shafer *et al.*, Emergent chirality in the electric polarization texture of titanate superlattices, Proc. Natl. Acad. Sci. U.S.A. **115**, 915 (2018).

[27] Y. Tikhonov *et al.*, Controllable skyrmion chirality in ferroelectrics, Sci. Rep. **10**, 8657 (2020).

[28] R. Ramesh and D. G. Schlom, Creating emergent phenomena in oxide superlattices, Nat. Rev. Mater. **4**, 257 (2019).

[29] X. Li *et al.*, Atomic-scale observations of electrical and mechanical manipulation of topological polar flux closure, Proc. Natl. Acad. Sci. U.S.A. **117**, 18954 (2020).

[30] K. Du, M. Zhang, C. Dai, Z. N. Zhou, Y. W. Xie, Z. H. Ren, H. Tian, L. Q. Chen, G. Van Tendeloo, and Z. Zhang, Manipulating topological transformations of polar structures through real-time observation of the dynamic polarization evolution, Nat. Commun. **10**, 4864 (2019).

[31] P. Chen *et al.*, Atomic imaging of mechanically induced topological transition of ferroelectric vortices, Nat. Commun. **11**, 1840 (2020).

[32] P. Chen *et al.*, Electrically driven motion, destruction, and chirality change of polar vortices in oxide superlattices, Sci. China Phys. Mech. Astron. **65**, 237011 (2022).

[33] A. R. Damodaran *et al.*, Phase coexistence and electric-field control of toroidal order in oxide superlattices, Nat. Mater. **16**, 1003 (2017).

[34] V. Stoica *et al.*, Optical creation of a supercrystal with three-dimensional nanoscale periodicity, Nat. Mater. **18**, 377 (2019).

[35] Q. Li *et al.*, Subterahertz collective dynamics of polar vortices, Nature (London) **592**, 376 (2021).

[36] L. D. Landau and E. M. Lifshitz, *Course of Theoretical Physics* (Elsevier, 2013).

[37] Y.-T. Shao *et al.*, Emergent chirality in a polar meron to skyrmion phase transition, arXiv:2101.04545.

[38] B. K. Lai, I. Ponomareva, I. Naumov II, I. Kornev, H. Fu, L. Bellaiche, and G. J. Salamo, Electric-Field-Induced Domain Evolution in Ferroelectric Ultrathin Films, Phys. Rev. Lett. **96**, 137602 (2006).

[39] Z. Hong and L.-Q. Chen, Blowing polar skyrmion bubbles in oxide superlattices, Acta Mater. **152**, 155 (2018).

[40] L. Zhou, Y. Wu, S. Das, Y. Tang, C. Li, Y. Huang, H. Tian, L.-Q. Chen, and Z. Hong, Local manipulation of polar skyrmions and topological phase transitions, Matter Radiat. Extremes **5**, 1031 (2022).

[41] See Supplemental Material at http://link.aps.org/supplemental/10.1103/PhysRevLett.129.107601 for more details on experimental and simulation methods, and additional analysis and results, which includes Refs. [42–49].

[42] S. J. Pennycook and P. D. Nellist, *Scanning Transmission Electron Microscopy: Imaging and Analysis* (Springer Science & Business Media, New York, 2011).
[43] M. Weyland and D. A. Muller, Tuning the convergence angle for optimum STEM performance, arXiv:2008.12870.
[44] J. Wang, Y. Li, L.-Q. Chen, and T.-Y. Zhang, The effect of mechanical strains on the ferroelectric and dielectric properties of a model single crystal—Phase field simulation, Acta Mater. **53**, 2495 (2005).
[45] Y. Li, S. Hu, Z. Liu, and L. Chen, Effect of substrate constraint on the stability and evolution of ferroelectric domain structures in thin films, Acta Mater. **50**, 395 (2002).
[46] Y. Li, S. Hu, Z. Liu, and L. Chen, Effect of electrical boundary conditions on ferroelectric domain structures in thin films, Appl. Phys. Lett. **81**, 427 (2002).
[47] L.-Q. Chen, *Physics of Ferroelectrics: A Modern Perspective* (Springer, Berlin, Heidelberg, 2007), p. 363.
[48] J. Wang, S.-Q. Shi, L.-Q. Chen, Y. Li, and T.-Y. Zhang, Phase-field simulations of ferroelectric/ferroelastic polarization switching, Acta Mater. **52**, 749 (2004).
[49] L. Q. Chen and J. Shen, Applications of semi-implicit Fourier-spectral method to phase field equations, Comput. Phys. Commun. **108**, 147 (1998).
[50] N. Nagaosa and Y. Tokura, Topological properties and dynamics of magnetic skyrmions, Nat. Nanotechnol. **8**, 899 (2013).
[51] N. Romming, C. Hanneken, M. Menzel, J. E. Bickel, B. Wolter, K. von Bergmann, A. Kubetzka, and R. Wiesendanger, Writing and deleting single magnetic skyrmions, Science **341**, 636 (2013).
[52] C. T. Nelson *et al.*, Domain dynamics during ferroelectric switching, Science **334**, 968 (2011).
[53] P. Gao, C. T. Nelson, J. R. Jokisaari, S.-H. Baek, C. W. Bark, Y. Zhang, E. Wang, D. G. Schlom, C.-B. Eom, and X. Pan, Revealing the role of defects in ferroelectric switching with atomic resolution, Nat. Commun. **2**, 591 (2011).
[54] N. Balke, M. Gajek, A. K. Tagantsev, L. W. Martin, Y. H. Chu, R. Ramesh, and S. V. Kalinin, Direct observation of capacitor switching using planar electrodes, Adv. Funct. Mater. **20**, 3466 (2010).
[55] S. Sze, D. Coleman, Jr., and A. Loya, Current transport in metal-semiconductor-metal (MSM) structures, Solid·State Electron. **14**, 1209 (1971).
[56] W. Jiang *et al.*, Blowing magnetic skyrmion bubbles, Science **349**, 283 (2015).
[57] M. Dawber, A. Gruverman, and J. Scott, Skyrmion model of nano-domain nucleation in ferroelectrics and ferromagnets, J. Phys. Condens. Matter **18**, L71 (2006).
[58] S. Woo *et al.*, Observation of room-temperature magnetic skyrmions and their current-driven dynamics in ultrathin metallic ferromagnets, Nat. Mater. **15**, 501 (2016).
[59] W. Legrand, D. Maccariello, N. Reyren, K. Garcia, C. Moutafis, C. Moreau-Luchaire, S. Collin, K. Bouzehouane, V. Cros, and A. Fert, Room-temperature current-induced generation and motion of sub-100 nm skyrmions, Nano Lett. **17**, 2703 (2017).
[60] T. Schulz, R. Ritz, A. Bauer, M. Halder, M. Wagner, C. Franz, C. Pfleiderer, K. Everschor, M. Garst, and A. Rosch, Emergent electrodynamics of skyrmions in a chiral magnet, Nat. Phys. **8**, 301 (2012).